IMA Journal of Applied Mathematics (2024) **89**, 374–386
https://doi.org/10.1093/imamat/hxae014
Advance Access publication on 4 June 2024

Exact and numerical solutions of a free boundary problem with a reciprocal growth law

N.R. McDonald* and Samuel J. Harris
Department of Mathematics, University College London, Gower Street, London WC1E 6BT, UK
*Corresponding author: n.r.mcdonald@ucl.ac.uk

[Received on 13 June 2023; revised on 4 January 2024; accepted on 24 April 2024]

A two-dimensional free boundary problem is formulated in which the normal velocity of the boundary is proportional to the inverse of the gradient of a harmonic function T. The field T is defined in a simply connected region which includes the point at infinity where it has a logarithmic singularity. The growth problem in which the boundary expands outwards is formulated both in terms of the Schwarz function of the boundary and a Polubarinova–Galin equation for the conformal map of the region from the exterior of the unit disk. An expanding free boundary is shown to be stable and explicit solutions for growing ellipses and a class of polynomial lemniscates are derived. Numerical solution of the Polubarinova–Galin equation is used to compute the evolution of the boundary having other initial shapes.

Keywords: free boundary; Schwarz function; wildfire; lemniscate growth.

1. Introduction

Two-dimensional free boundary problems in which the shape of an interface separating regions with distinct properties and dynamics must be determined as part of the solution arise in a variety of applications including freezing, melting and dissolution (e.g. Cummings *et al.*, 1999; Rycroft & Bazant, 2016; Ladd *et al.*, 2020), biology (e.g. Waters *et al.*, 2012; Kim *et al.*, 2016), geophysics (e.g. Dallaston & Hewitt, 2014; Grodzki & Szymczak, 2019), industrial coating (e.g. Tuck *et al.*, 1983), vortex dynamics (e.g. Crowdy, 1999; Riccardi, 2020) and, of course, the considerable literature on nonlinear water waves (e.g. Vanden-Broeck, 2010). Their inherent nonlinearity pose challenges to their understanding, and even the classic example of the Hele–Shaw (or Laplacian growth) free boundary problem (e.g. Gustafsson & Vasiliev, 2009), where the normal velocity of the free boundary depends on the gradient of a harmonic function, continues to receive attention (e.g. Anjos *et al.*, 2018; Morrow *et al.*, 2019; Lustri *et al.*, 2020; Sakakibara *et al.*, 2022; Cuttle *et al.*, 2023). In this class of problem, the harmonic function typically has logarithmic singularities which can be thought of as sources and sinks which serve to drive the free boundary evolution. The free boundary problem formulated and solved in this work is similar, except that the normal velocity is inversely related to the gradient of the harmonic field, leading to markedly different properties to Laplacian growth. Lundberg & Totik (2013) considered the same reciprocal growth law and used arguments based on potential theory and Green's functions to show that polynomial lemniscates are exact solutions, leading them to use the description *'lemniscate growth'* for this free boundary problem. Generalized growth laws for other types of Laplacian growth problems are discussed in, for example, the problems in Niemeyer *et al.* (1984) and Gubiec & Szymczak (2008).

This work further develops lemniscate growth by formulating analytical and numerical approaches and solutions and discussing applications. In Section 2, the problem is formulated in two different ways: (i) in terms of the Schwarz function for the curve coinciding with the free boundary, and (ii) a

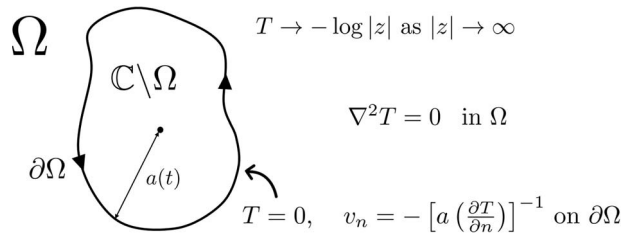

FIG. 1. Schematic diagram of the free boundary problem. T is a harmonic function in the exterior (infinite) domain Ω, and a is the conformal radius of the finite domain $\mathbb{C}\backslash\Omega$. The arrows on the boundary $\partial\Omega$ give the sense in which the arclength parameter s used in Section 2.1 increases.

Polubarinova–Galin equation for the conformal map from the exterior of the unit disk to the growing domain. In contrast to the Hele–Shaw problem, Section 3 shows that this growth problem (i.e. when the free boundary evolves by expanding towards infinity) is stable. The formulations are used in Section 4 to provide alternative derivations of the polynomial lemniscate solutions of Lundberg & Totik (2013) and, further, show that growing ellipses are also exact solutions. Section 5 presents a numerical scheme based on solving the Polubarinova–Galin equation which is used to find solutions for domains with a variety of different starting shapes. This section ends with some brief speculation on the application of the model to the spreading of wildfires, where the harmonic field is considered to be temperature and the free boundary marks the interface between burned and unburned regions of the fire. Section 6 gives the conclusion.

2. Formulation of the free boundary problem

Let Ω be the simply connected, infinite domain exterior to a smooth, non-intersecting, time-dependent closed curve $\partial\Omega(t)$ in the complex z-plane, where $z = x + \mathrm{i}y$. Suppose $T(x, y)$ is a harmonic function in Ω, such that $T \to -\log|z|$ as $|z| \to \infty$ and $T = 0$ on $\partial\Omega$. The free boundary $\partial\Omega(t)$ evolves according to

$$v_n = -\left[a\left(\frac{\partial T}{\partial n}\right)\right]^{-1}, \tag{2.1}$$

where v_n is the normal velocity of the curve and $a(t) > 0$ is the conformal radius of the finite domain $\mathbb{C}\backslash\Omega$. The problem is displayed diagrammatically in Fig. 1. The conformal radius is related to the logarithmic capacity (e.g. Baddoo & Trefethen, 2021) of the domain Ω and is the leading order term in the conformal map from the exterior of the unit ζ-disk to Ω i.e. $z \sim a\zeta$ as $z, \zeta \to \infty$. The direction of the normal is taken to be pointing into the domain Ω e.g. towards infinity when $\partial\Omega$ is a circle.

The posing of the normal velocity of the boundary proportional to the inverse of the normal gradient of T is the unusual feature here; Hele–Shaw free boundary problems, for example, would have $v_n = \partial_n T$ on $\partial\Omega$, and T would be identified as the real velocity potential. In this work, the boundary conditions on T imply the gradient of T in the normal direction is negative so that the rule (2.1) leads to growth in the sense that the areas of the finite domain $\mathbb{C}\backslash\Omega$ increases in time. As will be shown in Section 3, such growth is stable. The dependency of (2.1) on the time-varying conformal radius $a(t)$, which gives a measure of the size of the finite domain $\mathbb{C}\backslash\Omega$, slows the rate of growth of $\partial\Omega(t)$ as $a(t)$ increases. Note

that $a(t)$ is a parameter determined by the dynamics, and its presence effectively amounts to a rescaling of time. Its inclusion is not necessary in deriving exact and numerical solutions. It does, for example, prevent exponential growth in time of the radius of circular free boundaries which makes for a more realistic growth law when applied to problems such as wildfire spread (Section 5.2). Thus, this rescaling in $a(t)$ is included here.

2.1 *Formulation in terms of the Schwarz function*

The Schwarz function $S(z)$ of the curve $\partial\Omega$ in the z-plane is the unique function analytic in the neighbourhood of $\partial\Omega$ and such that $S(z) = \bar{z}$ on $\partial\Omega$ (Davis, 1974). Representing curves in the z-plane using $S(z)$ has proved successful in obtaining exact solutions for a range of free boundary problems including those of the Hele–Shaw class (e.g. Howison, 1992; Mineev-Weinstein *et al.*, 2000; Gustafsson & Vasiliev, 2009), 2D vortex dynamics, (e.g. Saffman, 1993; Crowdy, 1999; Riccardi, 2020), industrial coating flows (e.g. Johnson & McDonald, 2009; Marshall, 2011), water waves with vorticity (Crowdy, 2023) and curve-shortening (McDonald, 2022).

Letting s be the arclength parameter of $\partial\Omega$, it can be shown (e.g. Davis, 1974) that a geometric property of the Schwarz function is $dz/ds = 1/\sqrt{S_z}$, where the subscript z denotes differentiation with respect to z. Here and below, the branch of the square root is chosen to have negative imaginary part in order to be consistent with the parameter s increasing when going anti-clockwise around $\partial\Omega$. For an evolving curve $S = S(z,t)$, the normal velocity v_n at point z on $\partial\Omega$ is (e.g. Mineev-Weinstein *et al.*, 2000)

$$v_n = -\frac{\mathrm{i}}{2}\frac{\dot{S}}{\sqrt{S_z}}, \tag{2.2}$$

where $\dot{S}$ is the partial derivative of S with respect to time t. Let W be a function analytic in Ω such that $W = T + \mathrm{i}R$. Since $T = 0$ on $\partial\Omega$

$$\frac{\partial W}{\partial s} = \mathrm{i}\frac{\partial R}{\partial s} = \mathrm{i}\frac{\partial T}{\partial n} = -\frac{\mathrm{i}}{a v_n}, \tag{2.3}$$

where a Cauchy–Riemann equation and (2.1) have been used. Also, because W is an analytic function,

$$\frac{\partial W}{\partial s} = \frac{\partial W}{\partial z}\frac{\partial z}{\partial s} = \frac{1}{\sqrt{S_z}}\frac{\partial W}{\partial z}, \tag{2.4}$$

where the geometric property of the Schwarz function noted above has been used. Combining (2.2), (2.3) and (2.4) gives $\partial\Omega$

$$2\frac{\partial S}{\partial z} = a\dot{S}\frac{\partial W}{\partial z}. \tag{2.5}$$

It is interesting to compare (2.5) with the equivalent equation arising in Hele–Shaw free boundary flow (e.g. Howison, 1992; Gustafsson & Vasiliev, 2009), namely $\dot{S} = -2\partial_z F$, where $F(z)$ is the complex hydrodynamic potential incorporating driving sources or sinks. As in the Hele–Shaw case it is important to note that while (2.5) holds on $\partial\Omega$, by analytic continuation it holds in Ω and, in particular, the singular

behaviour of both sides of (2.5) must match as $z \to \infty$. This property is used in Section 4 to derive explicit solutions for the growth problem.

2.2 *Formulation as a Polubarinova–Galin-type equation*

In this subsection a Polubarinova–Galin-type equation (e.g. Howison, 1992; Gustafsson & Vasiliev, 2009) for the conformal map $z = f(\zeta, t)$ from the exterior of the unit disk in the ζ-plane to Ω is found. In addition to Hele–Shaw free boundary problems, such equations have proved effective in finding exact solutions for other two-dimensional free boundary problems including freezing and melting (e.g. Cummings *et al.*, 1999; Rycroft & Bazant, 2016), and as a basis for the numerical treatment of Hele–Shaw flow with and without surface tension (Dallaston & McCue, 2013).

In the z-plane the unit normal to $\partial\Omega$ has complex form $n = \zeta f'/|f'|$, where the dash indicates partial differentiation with respect to ζ. Thus the normal velocity on $\partial\Omega$ is

$$v_n = \mathrm{Re}\left[\dot{f}\frac{\overline{\zeta f'}}{|f'|}\right], \tag{2.6}$$

where the overbar represents taking the complex conjugate. Evaluating the normal velocity from (2.1) gives

$$\begin{aligned} v_n &= -\left[\frac{a}{2}\left(\frac{\partial(W+\overline{W})}{\partial n}\right)\right]^{-1} \\ &= -\left[\frac{a}{2}\mathrm{Re}\left(n\overline{\nabla}(W+\overline{W})\right)\right]^{-1} \\ &= -\left[a\,\mathrm{Re}\left(n\frac{\partial}{\partial z}(W+\overline{W})\right)\right]^{-1}, \\ &= -\left[a\,\mathrm{Re}\left(n\frac{\partial W}{\partial z}\right)\right]^{-1}. \end{aligned} \tag{2.7}$$

In the above equation, the equivalence $\overline{\nabla} \equiv \partial_x - \mathrm{i}\partial_y = 2\partial_z$ has been used, as has the fact that $W(z)$ is an analytic function. In the ζ-plane, $W = -\log\zeta$ and hence $W_z = -(\zeta f')^{-1}$ and upon equating (2.6) and (2.7) gives $|\zeta| = 1$

$$a\,\mathrm{Re}\left[\dot{f}\overline{\zeta f'}\right] = |f'|^2. \tag{2.8}$$

For comparison, in the Hele–Shaw case with a source of strength Q at the origin within a finite blob of fluid, the Polubarinova–Galin equation is $\mathrm{Re}\left[\dot{f}\overline{\zeta f'}\right] = Q$ with the sign of Q determining whether the free boundary of the fluid blob expands or contracts.

3. Stability

To begin, it is shown that $\partial\Omega(t)$ in the form of a circle with radius growing linearly in t is an exact solution. A circle of radius $a(t)$ centred at the origin has Schwarz function $S(z) = a^2/z$. Note that $a(t)$

is also the conformal radius appearing in (2.5). Substituting $S(z)$ into (2.5), using $\dot{S} = 2a\dot{a}/z$ and taking the limit $z \to \infty$ where it is known $W \to -\log z$, gives $\dot{a} = 1$. Hence $a = a_0 + t$ where a_0 is the initial radius of $\partial\Omega$.

Alternatively, the Polubarinova–Galin-type equation (2.8) can be used to derive the same solution: note the map from the ζ- to the z-plane is $z = f(\zeta, t) = a(t)\zeta$ and substituting this directly into (2.8) and using $\overline{\zeta} = 1/\zeta$ on $|\zeta| = 1$ also gives $\dot{a} = 1$.

To investigate the stability of the circular free boundary consider a perturbed interface and harmonic field T of the form

$$R = a + \delta_n \cos n\theta, \quad T = -\log\left(\frac{R}{a}\right) + \beta_n \left(\frac{a}{R}\right)^n \cos n\theta, \quad n = 1, 2, \cdots, \tag{3.1}$$

where $\delta_n(t) \ll a$ and $\beta_n(t) \ll 1$ are small time-varying amplitudes of the perturbation.

Since $T = 0$ on $R = a + \delta_n \cos n\theta$ it follows from (3.1) that to leading order $\delta_n = a\beta_n$. Also to leading order (2.1) gives

$$\dot{a} + \dot{\delta}_n \cos n\theta = \left(\frac{a}{R} + n\beta_n \frac{a^{n+1}}{R^{n+1}} \cos n\theta\right)^{-1}. \tag{3.2}$$

Putting $R = a + \delta_n \cos n\theta$ in (3.2) and simplifying gives, as expected, to leading order $\dot{a} = 1$ and to next order

$$\dot{\delta}_n = \frac{\delta_n}{a}(1 - n). \tag{3.3}$$

Stability demands that δ_n/a decreases with time or, equivalently, $\dot{\delta}_n/\delta - \dot{a}/a$ is negative (e.g. Dallaston & Hewitt, 2014). Using (3.3), it follows that $\dot{\delta}_n/\delta - \dot{a}/a = -n/a$ implying that the growth is stable. The above stability analysis of interface growth appears to be new, though the general stability of Laplacian growth problems where $v_n \sim |\nabla T|^\eta$ at the interface with $\eta < 0$ (note, $\eta = -1$ in this work) is noted in Gubiec & Szymczak (2008). The problem is time reversible (as noted in Lundberg & Totik, 2013), but is unstable since the sign of the RHS of (3.3) changes.

4. Exact solutions for the growth problem

In addition to the trivial solution of Section 2 when $\partial\Omega$ is a growing circle, two classes of exact solutions are derived in this section: ellipses and a class of polynomial lemniscates. Three examples of exact solutions are given in Fig. 2.

4.1 *Ellipse*

Let $z = f(\zeta, t) = c\zeta + d/\zeta$, where $c(t)$ and $d(t)$ are real, time-varying parameters, be the conformal map from the exterior of the unit ζ-disk to the exterior of an ellipse with axes of length $|c + d|$ and $|c - d|$. Substituting $f(\zeta, t)$ into (2.8) and letting $\zeta = \exp(\mathrm{i}\theta)$ gives terms which are either θ-independent or

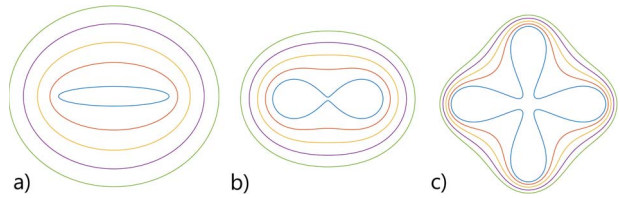

FIG. 2. (a) Growth of an elliptical boundary according to (4.5) with $c_0 = 1$ and $d_0 = 0.7$, with plots of $\partial\Omega$ shown at equal time intervals between $t = 0$ and $t = 2$. (b) Growth of a Cassini oval $|z^2 - 1| = e^2$ with $e = t + 1.001$ between $t = 0$ and $t = 1$. (c) Growth of the lemniscate $|z^4 - 1| = e^4$ with $e(0) = 1.0001$ between $t = 0$ and $t = 0.25$.

linear in $\cos 2\theta$. Equating like terms gives two ODEs for the unknown coefficients c and d:

$$\begin{aligned} a\left(c\dot{c} - \dot{d}d\right) &= c^2 + d^2, \\ a\left(c\dot{d} - d\dot{c}\right) &= -2cd. \end{aligned} \tag{4.1}$$

An alternative derivation of (4.1) uses the Schwarz function. First, note that by taking the conjugate of $z = c\zeta + d/\zeta$ and using $\overline{\zeta} = \zeta^{-1}$ on $\partial\Omega$, it follows in the limit $z \to \infty$

$$S = \frac{d}{c}z + \frac{c^2 - d^2}{z} + \cdots, \quad z \to \infty. \tag{4.2}$$

Next, since $W = -\log\zeta$,

$$W = -\log\left(\frac{z}{c}\right) + \frac{cd}{z^2} + \cdots, \quad z \to \infty. \tag{4.3}$$

Substituting (4.2) and (4.3) into (2.5) gives to $\mathcal{O}(1)$ and $\mathcal{O}(z^{-2})$

$$\begin{aligned} a\frac{d}{dt}\left(\frac{d}{c}\right) &= -2\frac{d}{c}, \\ a\left[\frac{d}{dt}(c^2 - d^2) + 2cd\frac{d}{dt}\left(\frac{d}{c}\right)\right] &= 2(c^2 - d^2), \end{aligned} \tag{4.4}$$

which can be shown to be equivalent to (4.1).

Since the conformal radius of the map f is c, then $a \equiv c$ and the system (4.1) has solution

$$c = t + c_0, \quad d = \frac{c_0 d_0}{t + c_0}, \tag{4.5}$$

where $c(0) = c_0$ and $d(0) = d_0$. Thus the ellipse grows becoming more circular as the ratio $|d/c|$ decreases with increasing time t. An example with $c_0 = 1$ and $d_0 = 0.7$ is shown in Fig. 2a.

4.2 *Cassini oval and polynomial lemniscates*

Let $\partial\Omega$ be a Cassini oval, an example of a polynomial lemniscate, given by $|z^2-1|=e^2$, where $e>1$. The conformal map from the exterior of the unit ζ-disk to the exterior of the Cassini oval is (Symm, 1967)

$$z=\sqrt{e^2\zeta^2+1}. \tag{4.6}$$

The leading order term in the expansion of (4.6) as $\zeta\to\infty$ is $e\zeta$ showing that the conformal radius $a\equiv e$. Direct substitution of (4.6) into (2.8) putting $\zeta=\exp(\mathrm{i}\theta)$ shows that it is an exact solution provided $\dot{e}=1$ and so $e(t)=t+e_0$, where $e_0=e(0)>1$.

Alternatively, the same result for $e(t)$ can be obtained using the Schwarz function equation (2.5): begin by noting

$$|z^2-1|=e^2 \implies |z^2-1|^2=e^4 \quad \text{or} \quad S^2=1+\frac{e^4}{z^2-1}. \tag{4.7}$$

From (4.7), to leading order as $z\to\infty$, $S^2\to 1+e^4/z^2$, and hence $\dot{S}\to 2e^3\dot{e}/z^2$ and $S_z\to -e^4/z^3$. But it is known that as $z\to\infty$, $W\to -\log z$ and so (2.5) with $a\equiv e$ gives, after simplification, $\dot{e}=1$, as found via the Polubarinova–Galin equation (2.8) approach. Figure 2b shows a growing Cassini oval.

That the Cassini oval is an exact solution is expected since it is a type of polynomial lemniscate: Lundberg & Totik (2013) show that the reciprocal growth law of the type (2.1) (in the absence of the conformal radius a which only affects the timescale of the evolution) preserves polynomial lemniscates. In fact, for polynomial lemniscates of the form $|z^M-1|=e^M$, $M=2,3,\cdots$, the above steps can be followed to show $\dot{e}=e/a$. With the realisation that the conformal map from the exterior of the unit ζ-disk to Ω is $z=\sqrt[M]{e^M\zeta^M+1}$, it follows that the conformal radius $a\equiv e$ and so $\dot{e}=1$ for $M=2,3,\cdots$. Figure 2c shows an example of the growth of the lemniscate $|z^4-1|=e^4$ with $e(0)=1.0001$.

5. Numerical procedure, examples and application to wildfire spread

5.1 *Numerical method and results*

The shape of a more general $\partial\Omega(t)$ is found by solving (2.8) numerically to find the map from the exterior of the unit ζ-disk to Ω. The numerical procedure is based on the method in Dallaston & McCue (2013, 2016) and begins by writing the general form of the conformal map as a Laurent series

$$z=f(\zeta,t)=a(t)\zeta+\sum_{k=0}^{\infty}c_k(t)\zeta^{-k}, \tag{5.1}$$

where, with no loss of generality, the conformal radius $a(t)>0$ is real, and $c_k(t)=a_k(t)+ib_k(t)$ are complex functions in time. The numerical task is to determine the unknown coefficients in (5.1) and is done approximately by truncating the series at N terms, giving $n=2(N+1)+1=2N+3$ unknown real functions in time: $a(t)$, $a_k(t)$, $b_k(t)$, $k=0,1,\cdots,N$. Selecting n equally spaced points around the unit ζ-disk, the Polubarinova–Galin (PG) equation (2.8) becomes a system of n coupled ODEs determining the time evolution of the n Laurent coefficients. The ODE system is solved using the MATLAB routine *ode*15*i*.

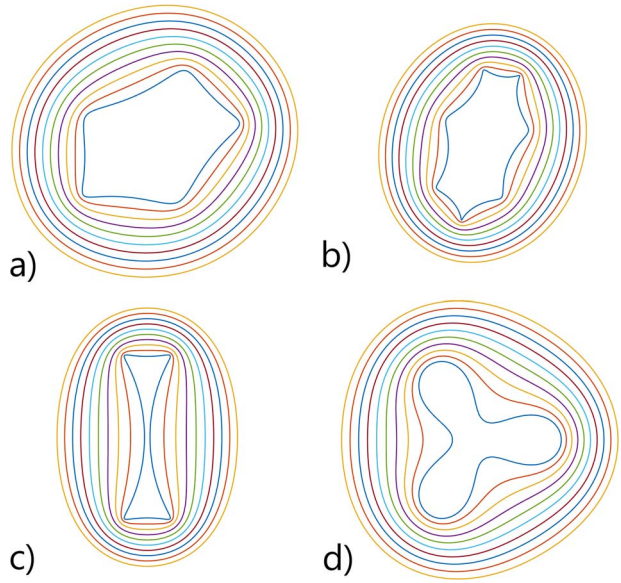

FIG. 3. Growth of various shapes from $t = 0$ to $t = 1$ with Laurent series truncation $N = 128$, (a) irregular pentagon, (b) irregular object, (c) hourglass. (d) A lemniscate with $e(0) = 1.01$, $M = 3$ and $N = 256$.

The numerical method is tested by comparing results with the exact solutions of (2.1). The ellipse has a conformal map immediately in the form of (5.1): $z = a(t)\zeta + c_1(t)\zeta^{-1}$. The map of the general polynomial lemniscate of degree M can also be written as a Laurent series

$$z = (e^M\zeta^M + 1)^{1/M} = e\zeta + \sum_{k=1}^{\infty} \binom{1/M}{k} (e\zeta)^{1-kM}, \tag{5.2}$$

where the identification $a(t) = e(t)$ is made. The same set of points around the ζ-disk is mapped using both the numerical and exact solutions for z, allowing for direct comparison. It is found that the distance between corresponding exact and numerical points has a relative error of $\mathcal{O}(10^{-7})$ at any time during the simulation.

Figure 3 gives examples of the evolution of the free boundary under (2.1) for a variety of shapes: an irregular pentagon, an irregular object, an hourglass—all with Laurent series truncation $N = 128$—and the lemniscate $|z^3 - 1| = e^3$ with $e(0) = 1.01$, $M = 3$ and $N = 256$. The Laurent coefficients at $t = 0$ of these shapes (excluding the lemniscate) are taken from Rycroft & Bazant (2016)—see their figures 5a, 2f and 7a. In all plots, concave and convex regions are 'smoothed out' as each shape approaches a growing circle. The timescale to which it reaches a circular shape (within some level of approximation) depends on the initial shape; while the irregular pentagon has almost reached a circle in Fig. 3a, the hourglass remains notably non-circular at $t = 1$ in Fig. 3c.

Many shapes, at least initially, are not well approximated by a truncated version of the Laurent series (5.1). In such cases, the numerical approach is modified as follows: the conformal map of the initial, arbitrary shape can be found numerically using the Schwarz–Christoffel (SC) Toolbox (Driscoll, 1996). The Toolbox function *extermap* is used, which finds the map $g(\zeta)$ from the *interior* of the unit

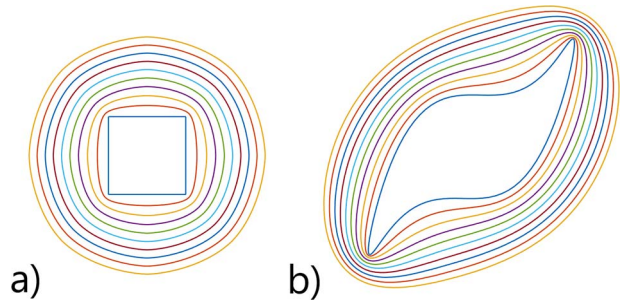

FIG. 4. Growth of various shapes from $t = 0$ to $t = 1$ with series truncation $N = 128$, (a) a square, (b) a blade.

ζ-disk to the exterior Ω of the free boundary. Then, a power series in ζ is added to the initial map g as follows:

$$z = f(\zeta, t) = a^*(t)g(\zeta) + \sum_{k=0}^{\infty} c_k(t)\zeta^k, \tag{5.3}$$

where $a^*(0) = 1$ and $c_k(0) = 0$, $\forall k$. Note that (i) the series powers are opposite in sign from (5.1), to accommodate the map $g(\zeta)$ being from the interior of the ζ-disk, and (ii) the conformal radius is now $a(t) = a^*(t)A$, where A is the conformal radius of the map $g(\zeta)$.

As before, the series (5.3) is truncated at N terms and solved using *ode*15*i*. Note the SC Toolbox need only be used once at the start of the numerical simulation. Figure 4 shows the evolution of two shapes found using this method: a square and a blade (e.g. Gopal & Trefethen, 2019), which both expand and smooth towards a circular shape, as expected.

The numerical method can also be used to find solutions to a more general growth law

$$v_n = -\left[a\left(\frac{\partial T}{\partial n}\right)\right]^{-\alpha}, \tag{5.4}$$

where the constant $\alpha > 0$ is chosen to be positive for stability. In this case, the PG equation becomes

$$a^{\alpha}\,\mathrm{Re}\left[\dot{f}\overline{\zeta f'}\right] = |f'|^{1+\alpha}. \tag{5.5}$$

It is straightforward to show that a circle with $\dot{a} = 1$ is an exact solution of (5.5) $\forall\alpha$. However, additional exact solutions (e.g. ellipses, lemniscates) have not been found for $\alpha \neq 1$. Figure 5 shows the evolution of an hourglass with Laurent series truncation $N = 128$ from $t = 0$ to $t = 1$ under different values of α: 0.1, 0.5, 1 and 2. It is observed that, for larger values of α, the hourglass evolves into a circular shape more quickly than for smaller values. Comparing Fig. 5a and 5d shows this most clearly: the final free boundary shape in Figure 5a still resembles the initial hourglass shape, whereas the final shape of Fig. 5d is almost a circle.

5.2 *Relation to the spread of wildfires*

The increasing prevalence and danger of wildfires globally has led to a renewed effort in understanding their complex behaviour and interactions with the atmosphere and the environment—see the recent

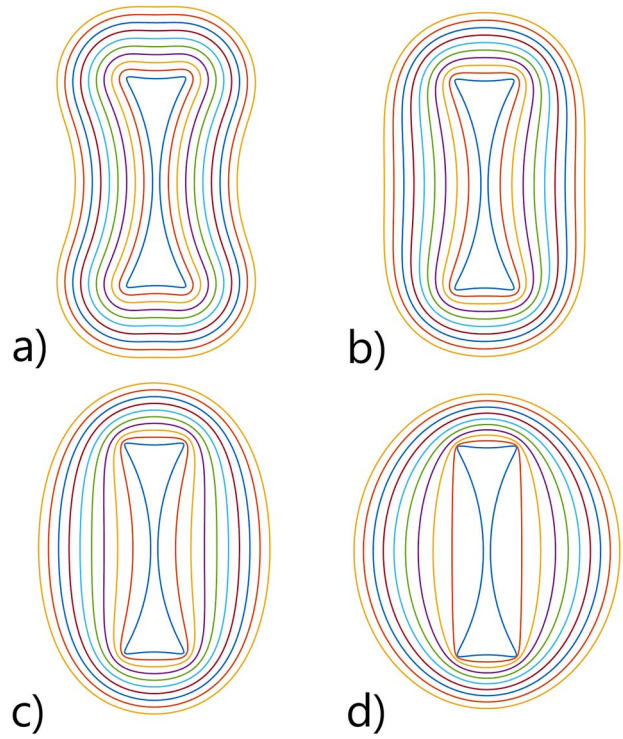

FIG. 5. Growth of an hourglass from $t = 0$ to $t = 1$, series truncation $N = 128$, under the general growth law (5.5) where (a) $\alpha = 0.1$, (b) $\alpha = 0.5$, (c) $\alpha = 1$, (d) $\alpha = 2$.

review article (Silva *et al.*, 2022). A fundamental task is determining the evolution of the fire perimeter, or fire line: the interface between burned and unburned regions. Convection and radiation are the principal candidates for driving this evolution, with their combined effects often modelled by a constant normal velocity, or rate of spread (ROS), of the fire line (e.g. Hilton *et al.*, 2016, 2018; Harris & McDonald, 2022). Mathematically, this can be considered a free boundary problem with the fire line evolution determined as part of the solution of the PDE system governing the wildfire dynamics. It is worth speculating on the relevance in applying the free boundary problem of this work to wildfires in this way. There are two appealing features in doing so.

First, the model does not impose an ad-hoc constant ROS; rather the ROS is deterministic, depending on the gradient of the harmonic function T in Ω (the unburned region) via the growth law (2.1). The quantity T can be thought of as temperature which is hottest $T = 0$ at the fire line $\partial\Omega$: the ignition temperature of the fuel. Away from the fire line, the temperature decreases such that $T \to -\infty$ as $r \to \infty$. Although this unbounded limit in T is physically unrealistic, the slow logarithmic decay in T close to the fire line is the important property in this model. Since T is harmonic, its behaviour can be interpreted physically as the diffusion of heat. While it should be cautioned that there is no observational evidence that wildfires are driven diffusively, some wildfire models do explicitly include diffusive terms for heat in the vicinity of the fire line, see e.g. Weber (1991).

Second, the model reproduces an enhanced ROS near concave regions of the fire line in comparison with convex regions, a property commonly observed in wildfire evolution but often attributed to ad-hoc

effects such as fire line curvature or fire-induced winds (e.g. Hilton *et al.*, 2016, 2018). This property is evident in Figs 2c and 3 with the fire line becoming more circular as time increases. Physically, the fire grows by intense (diffusive) heating of surrounding unburned fuel which warm until they reach the ignition temperature $T = 0$. Temperature contours in the unburned region are closer in convex regions, resulting in a larger heat gradient there. Since the fire line progresses to the contour $T = 0$ at the same instant, it does so at a greater normal velocity in the regions where the temperature gradient is less, as modelled by the reciprocal growth law. Other choices of $\alpha > 0$ (see (5.4)) also qualitatively reproduce this behaviour, thus further investigation is required to determine which choice of α best models the fire spread. Note the inclusion of the conformal radius factor in (2.1) does not affect the geometric evolution of the free boundary. This implies that in the absence of other effects such as wind, the rate of change of the conformal radius with time is constant. Thus, for a circular wildfire, the ROS is constant as supposed in e.g. Anderson *et al.* (1982); Hilton *et al.* (2016, 2018).

6. Conclusion

Explicit solutions are found for a free boundary growth problem in which the normal velocity of elliptical or lemniscatic boundaries is the reciprocal of the gradient of a harmonic function with a logarithmic singularity at infinity. The methods are based on either the Schwarz function formulation of the free boundary problem, or the Polubarinova–Galin equation for the conformal map from the growth domain to the exterior of the unit disk. The latter method additionally provides the basis for a numerical approach, enabling the evolution of more general initial shapes, and more general growth laws, to be computed.

It is speculated that the free boundary problem bears some resemblance to the growth of wildfires in that it reproduces the behaviour of convex and concave portions of the fire boundary. It also provides a dynamic model for the ROS of the fire line. Further research is required to assess its relevance, including comparison with wildfire experiments and observations.

Further work focusing on multiply connected domains is of interest. In this respect, note that lemniscates of Section 4.2 with $0 < e < 1$ have disconnected boundaries and that increasing e represents the growth and eventual merger of initially near-circular blobs. In wildfire modelling, the merger of fires, including spot fires, is of particular interest (e.g. Storey *et al.*, 2021).

Acknowledgments

The authors thank the reviewers for their helpful comments.

Funding

Funding UK Engineering and Physical Sciences Research Council PhD studentship (Grant No. EP/N509577/1 and EP/T517793/1 to S.J.H.).

Conflict of Interest

There are no conflicts of interest for all authors.

References

Anderson, D. H., Catchpole, E. A., De Mestre, N. J. & Parkes, T. (1982) Modelling the spread of grass fires. *ANZIAM J.*, **23**, 451–466.

Anjos, P. H. A., Dias, E. O. & Miranda, J. A. (2018) Fingering instability transition in radially tapered Hele-Shaw cells: insights at the onset of nonlinear effects. *Phys. Rev. Fluids*, **3**, 124004.

Baddoo, P. & Trefethen, L. N. (2021) Log-lightning computation of capacity and Green's function. *Maple Trans.*, **1**, 14124:1–14124:13.

Crowdy, D. (1999) A class of exact multipolar vortices. *Phys. Fluids*, **11**, 2556–2564.

Crowdy, D. G. (2023) Exact solutions for steadily travelling water waves with submerged point vortices. *J. Fluid Mech.*, **954**, A47.

Cummings, L. M., Hohlov, Y. E., Howison, S. D. & Kornev, K. (1999) Two-dimensional solidification and melting in potential flows. *J. Fluid Mech.*, **378**, 1–18.

Cuttle, C., Morrow, L. C. & MacMinn, C. W. (2023) Compression-driven viscous fingering in a radial Hele-Shaw cell. *Phys. Rev. Fluids*, **8**, 113904.

Dallaston, M. C. & Hewitt, I. J. (2014) Free-boundary models of a meltwater conduit. *Phys. Fluids*, **26**, 083101.

Dallaston, M. C. & McCue, S. W. (2013) An accurate numerical scheme for the contraction of a bubble in a Hele-Shaw cell. *ANZIAM J.*, **54**, C309–C326.

Dallaston, M. C. & McCue, S. W. (2016) A curve shortening flow rule for closed embedded plane curves with a prescribed rate of change in enclosed area. *Proc. Roy. Soc. A*, **472**, 20150629.

Davis, P. J. (1974) *The Schwarz Function and its Applications*. Washington, USA: Math. Assoc. America.

Driscoll, T. (1996) Algorithm 756: a MATLAB toolbox for Schwarz-Christoffel mapping. *ACM Trans. Math. Softw.*, **22**, 168–186.

Gopal, A. & Trefethen, L. (2019) Representation of conformal maps by rational functions. *Numer. Math.*, **142**, 359–382.

Grodzki, P. & Szymczak, P. (2019) Reactive-infiltration instability in radial geometry: from dissolution fingers to star patterns. *Phys. Rev. E (3)*, **100**, 033108.

Gubiec, T. & Szymczak, P. (2008) Fingered growth in channel geometry: a Loewner-equation approach. *Phys. Rev. E (3)*, **77**, 041602.

Gustafsson, B. & Vasiliev, A. (2009) *Conformal and Potential Analysis in Hele-Shaw Cells*. Basel: Birkhauser.

Harris, S. J. & McDonald, N. R. (2022) Fingering instability in wildfire fronts. *J. Fluid Mech.*, **943**, A34.

Hilton, J., Miller, C., Sharples, J. & Sullivan, A. (2016) Curvature effects in the dynamic propagation of wildfires. *Int. J. Wildland Fire*, **25**, 1238–1251.

Hilton, J., Sullivan, A., Swedosh, W., Sharples, J. & Thomas, C. (2018) Incorporating convective feedback in wildfire simulations using pyrogenic potential. *Environ. Model. Softw.*, **107**, 12–24.

Howison, S. D. (1992) Complex variable methods in Hele-Shaw moving boundary problems. *European J. Appl. Math.*, **3**, 209–224.

Johnson, E. R. & McDonald, N. R. (2009) Necking in coating flow over periodic substrates. *J. Engrg. Math.*, **65**, 171–178.

Kim, I. C., Perthame, B. & Souganidis, P. E. (2016) Free boundary problems for tumor growth: a viscosity solutions approach. *Nonlinear Anal.*, **138**, 207–228.

Ladd, A., Yu, L. & Szymczak, P. (2020) Dissolution of a cylindrical disk in Hele-Shaw flow: a conformal-mapping approach. *J. Fluid Mech.*, **903**, A46.

Lundberg, E. & Totik, V. (2013) Lemniscate growth. *Analysis Math. Phys.*, **3**, 45–62.

Lustri, C. J., Green, C. C. & McCue, S. W. (2020) Selection of a Hele-Shaw bubble via exponential asymptotics. *SIAM J. Appl. Math.*, **80**, 289–311.

Marshall, J. S. (2011) Steady uniform vortex patches around an assembly of walls or flat plates. *Quart. J. Mech. Appl. Math.*, **65**, 27–60.

McDonald, N. R. (2022) The fundamental solutions of the curve shortening problem via the Schwarz function. *Complex Analysis Syn.*, **8**, article 5, 1–6.

Mineev-Weinstein, M., Wiegmann, P. B. & Zabrodin, A. (2000) Integrable structure of interface dynamics. *Phys. Rev. Lett.*, **84**, 5106–5109.

Morrow, L. C., Moroney, T. J. & McCue, S. W. (2019) Numerical investigation of controlling interfacial instabilities in non-standard Hele-Shaw configurations. *J. Fluid Mech.*, **877**, 1063–1097.

Niemeyer, L., Pietronero, L. & Wiesmann, H. J. (1984) Fractal dimension of dielectric breakdown. *Phys. Rev. Lett.*, **52**, 1033–1036.

Riccardi, G. (2020) Remarks on equilibria of two-dimensional uniform vortices with polygonal symmetry. *Eur. J. Mech. B/Fluids*, **83**, 1–14.

Rycroft, C. & Bazant, M. (2016) Asymmetric collapse by dissolution or melting in a uniform flow. *Proc. R. Soc. A.*, **472**, 20150531.

Saffman, P. G. (1993) *Vortex Dynamics*. Cambridge: Cambridge University Press.

Sakakibara, K., Shimoji, Y. & Yazaki, S. (2022) A simple numerical method for Hele-Shaw type problems by the method of fundamental solutions. *Japan J. Indust. Appl. Math.*, **39**, 869–887.

Silva, J., Marques, J., Gonçalves, I., Brito, R., Teixeira, S., Teixeira, J. & Alvelos, F. (2022) A systematic review and bibliometric analysis of wildland fire behavior modeling. *Fluids*, **7**, 374.

Storey, M. A., Price, O. F., Almeida, M., Ribeiro, C., Bradstock, R. A. & Sharples, J. J. (2021) Experiments on the influence of spot fire and topography interaction on fire rate of spread. *PLoS One*, **16**, e0245132.

Symm, G. T. (1967) Numerical mapping of exterior domains. *Numer. Math.*, **10**, 437–445.

Tuck, E. O., Bentwich, M. & Van Der Hoek, J. (1983) The free-boundary problem for gravity-driven unidirectional viscous flows. *IMA J. Appl. Math.*, **30**, 191–208.

Vanden-Broeck, J.-M. (2010) *Gravity–Capillary Free-Surface Flows*. Cambridge Monographs on Mechanics: Cambridge University Press.

Waters, A., Blanchette, F. & Kim, A. D. (2012) Modeling huddling penguins. *PLOS ONE*, **7**, e50277.

Weber, R. (1991) Modelling fire spread through fuel beds. *Prog. Energ. Combust. Sci.*, **17**, 67–82.